Dissipation measurements during ultrasonic fatigue tests

Antoine Blanche, Nicolas Ranc, Véronique Favier, André Chrysochoos

▶ **To cite this version:**

Antoine Blanche, Nicolas Ranc, Véronique Favier, André Chrysochoos. Dissipation measurements during ultrasonic fatigue tests. PhotoMechanics 2013, May 2013, Montpellier, France. pp.Clé USB. hal-00859821

HAL Id: hal-00859821
https://hal.science/hal-00859821v1

Submitted on 9 Sep 2013

HAL is a multi-disciplinary open access archive for the deposit and dissemination of scientific research documents, whether they are published or not. The documents may come from teaching and research institutions in France or abroad, or from public or private research centers.

L'archive ouverte pluridisciplinaire **HAL**, est destinée au dépôt et à la diffusion de documents scientifiques de niveau recherche, publiés ou non, émanant des établissements d'enseignement et de recherche français ou étrangers, des laboratoires publics ou privés.

DISSIPATION MEASUREMENTS DURING ULTRASONIC FATIGUE TESTS

A. Blanche[a,b], N. Ranc[b], V. Favier[b] and A. Chrysochoos[a]
a. Laboratoire de Mécanique et Génie Civil (LMGC), Université Montpellier 2,
CNRS, Place Eugène Bataillon, 34090 Montpellier, France
b. Laboratoire Procédés et Ingénierie en Mécanique et Matériaux (PIMM), UMR CNRS 8006
Arts et Métiers Paristech, 151 boulevard de l'Hôpital 75013 Paris, France
antoine.blanche@univ-montp2.fr

ABSTRACT: The aim of this paper is to analyse the dissipation observed during dynamic fatigue loading at low stress range and high number of cycles. Infrared thermographic techniques were developed to estimate the mean dissipation per cycle. Results derived from tests performed at high loading frequency on pure copper specimens showed a drift of dissipative regimes incompatible with concepts of fatigue limit and/or asymptotic cyclic stability.

1. INTRODUCTION

This paper presents an experimental calorimetric approach developed to measure dissipated energy during high and very high cycle fatigue (HCF & VHCF) loading. Fatigue tests were performed using a piezoelectric system. The loading frequency was about 20 kHz inducing dynamic deformation processes, the stress level remaining much lower than fatigue resistance. The use of higher loading frequencies than conventional frequencies (~ 30 Hz) brings advantages (1) to reach the HCF & VHCF regime within a reasonable time and (2) to increase intrinsic dissipation and thus to generate temperature variations which can be detect with the current thermal measurement devices. In the following, the experimental approach is briefly described. Then the infrared image processing developed to pass from infrared thermal data to 1D distribution of heat sources is presented. The heat diffusion model and the identification of the heat exchanges are shown. Finally some results extracted from experiments on pure cupper are given. They show that energy dissipation exists whatever the stress range we used. They also show an evolution of the dissipation intensity reflecting incompatible with the concept of plastic shakedown.

2. EXPERIMENTAL SETUP

The experimental setup involves the mechanical testing machine shown on Fig. 1. It essentially involves 3 components [1]:

- a piezoelectric system that transforms an electrical signal into a displacement
- an ultrasonic horn which amplifies this displacement (usually 3 to 9 times)
- a specimen screwed on the horn and free of stress at its bottom extremity

This dynamic loading system is designed, assuming an elastic behaviour, in order to have a longitudinal vibration mode at a frequency of around 20 kHz. In order to obtain the relation between the displacement variation on the horn edge and the input electrical signal, the testing machine is calibrated with a laser extensometer. It is then possible to derive the stress variation distribution along the specimen length (Fig. 2). The load ratio is $R_\sigma = \sigma_{min}/\sigma_{max} = -1$. The computation shows the following usual result in static situations, but no so obvious in dynamic situations: the lower the specimen cross-section the higher the stress level.

Specimens are in pure copper (Cu>99.95%) and the grain size is about 25 µm. The fatigue strength of this material is around 93 MPa after 10^{10} cycles [2,3]. During fatigue tests, an infrared camera (512x640 pixels) monitors the temperature field on the specimen surface. A pixel calibration is performed using a black body [4]. The specimen surface is painted in matte black to have a uniform surface emissivity close to 1. Spatial resolution is about 0.1 mm/pixel. From the temperature measurements, the intrinsic dissipation was determined using a 1D heat diffusion model (see the following section).

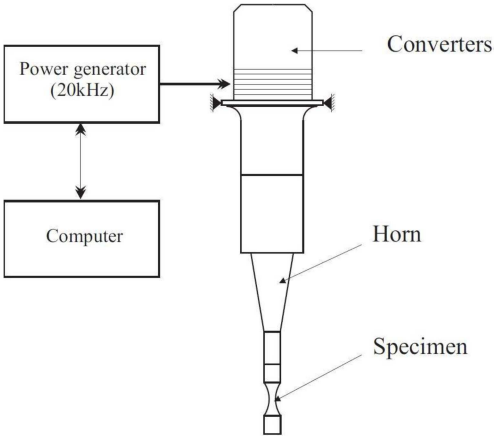

Figure 1- Scheme of the piezoelectric fatigue machine

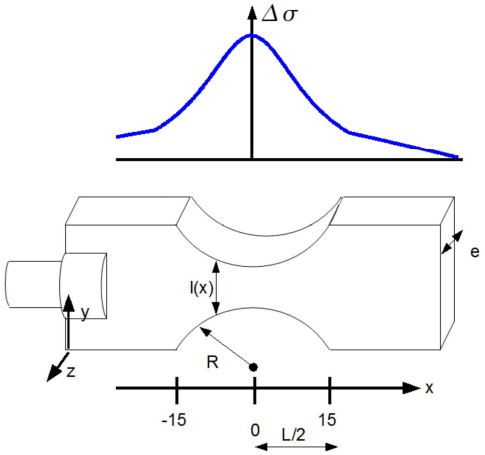

Figure 2- Stress distribution

3. CALORIMETRIC ANALYSIS

3.1 Heat diffusion model

A numerical model was built to estimate the evolution of intrinsic dissipation fields from the temperature measurement fields during the fatigue test. The paper focuses hereafter on the making of longitudinal distributions of heat sources within the specimen gage part. A 1D calorimetric analysis has been justified assuming in a first approximation a uniaxial tension-compression stress state.
From the heat equation:

$$\rho C\dot{T} - k\Delta T = s \tag{1}$$

where T is the temperature, ρ the mass density, C the heat capacity, k the thermal conduction coefficient and $s(x,y,z,t)$ symbolizes the volume heat source. Following classical hypotheses [5], the 1D diffusion equation for a non-constant cross-section can be written as [6]:

$$\rho C\left(\frac{\partial\bar{\bar{\theta}}}{\partial t}+\frac{\bar{\bar{\theta}}}{\tau_{th}^{1D}}\right)-k\left(\frac{\partial^2\bar{\bar{\theta}}}{\partial x^2}+\frac{\partial\bar{\bar{\theta}}}{\partial x}\frac{S'}{S}\right)=\bar{\bar{d}}_1+\bar{\bar{s}}_{the} \tag{2}$$

where the mean temperature variation over the cross-section $\bar{\bar{\theta}}(x,t)=T-T_0$ is identified with the surface temperature, S' being the first derivative of the cross-section S while $\bar{\bar{d}}_1(x,t)$ and $\bar{\bar{s}}_{the}(x,t)$ are the longitudinal profiles of dissipation and thermoelastic sources. Moreover the time constant τ_{th}^{1D} characterizes the lateral heat exchanges by conduction, convection and radiation between the specimen and the surroundings. These exchanges are assumed to be proportional to the temperature variation (linear Fourier boundary conditions). In order to estimate the left-hand side of Eq. (2), longitudinal temperature profiles were built by averaging the surface temperature over the specimen width.

Taking the loading frequency (20 kHz) and the maximum frame rate of the IR camera (100 Hz) into account (integration time = 1000 µs = 20 cycles), it must be stressed that the thermoelastic source amplitudes are, here, out of reach. Only the mean dissipation per cycle will be derived from the discrete, noisy thermal data.

3.2 Dissipation estimate

To compute d_1, the different partial derivative operators were estimated using spatio-temporal fitting. The local approximation functions were chosen as:

$$\theta^{app}(x,t)=P_1(x)t+P_2(x) \tag{3}$$

where $P_1(x)$ and $P_2(x)$ are second-order polynomials in x. These polynomials are identified over each approximation zone using a local least-squares method. The approximated thermal field is then used to compute the intrinsic dissipation, via an estimate of the time and space partial derivative operators of the heat equation (see Eq.2). The reader interested in this image processing method is referred to [5].

3.3 Thermal return

To show the relevance of the 1D thermal model, thermal returns were studied. In such a situation, no heat source occured and a pure diffusion problem could be analyzed. For 1D analysis, the partial differential problem is sum up in Eq.(4) where $\bar{\bar{\theta}}_{\exp}(x=\pm L/2,t)$ are the experimental Dirichlet boundary conditions, L being the length of the sample gage part (see Fig.1) :

$$\begin{aligned}&\rho C\left(\frac{\partial\bar{\bar{\theta}}}{\partial t}+\frac{\bar{\bar{\theta}}}{\tau_{th}^{1D}}\right)-k\left(\frac{\partial^2\bar{\bar{\theta}}}{\partial x^2}+\frac{\partial\bar{\bar{\theta}}}{\partial x}\frac{S'}{S}\right)=0\\&\bar{\bar{\theta}}(x,t=0)=\bar{\bar{\theta}}_{\exp}(x,t=0)\\&\bar{\bar{\theta}}(x=\pm L/2,t)=\bar{\bar{\theta}}_{\exp}(x=\pm L/2,t)\end{aligned} \tag{4}$$

Figure 3 shows different temperature profiles. The dissymmetry of boundary conditions comes from the fact that at one extremity the sample is fixed at the horn *(x=-L/2)* which is cooled by a cold air jet while the sample is totally free on the other side *(x=L/2)*. The comparison between assessments and predicted results derived from Eq.(4) is quasi perfect.

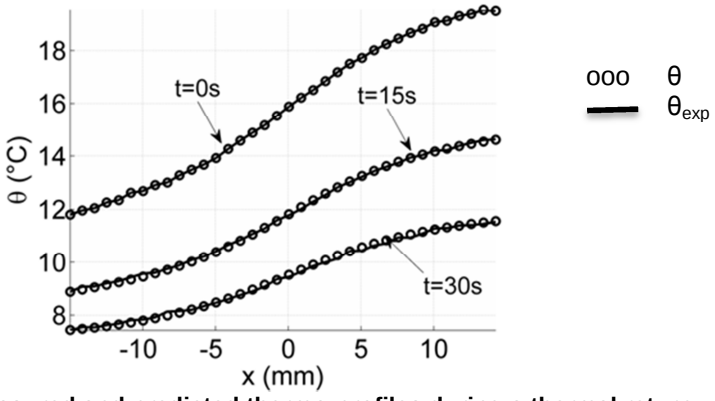

Figure 3- Measured and predicted thermo-profiles during a thermal return

4. RESULTS AND DISCUSSION

In the following, intrinsic dissipation d_1 is divided by ρC in order to have volume energy rate (W/m^3) expressed in (°C/s). Figure 4 and 5 show experimental results. Fatigue tests consisted in performing 10^6 cycles at different stress level (from 20 MPa to 90 MPa). Results stressed that dissipated energy exists whatever the applied load. Higher the stress range, higher the intrinsic dissipation. We can note that even below 34 MPa, sometimes considered as an "irreversible threshold" in the literature [2], a non-zero intrinsic dissipation can be detected.

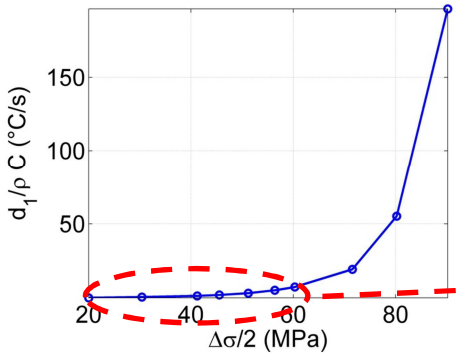

Figure 4- Dissipation vs. Stress amplitude

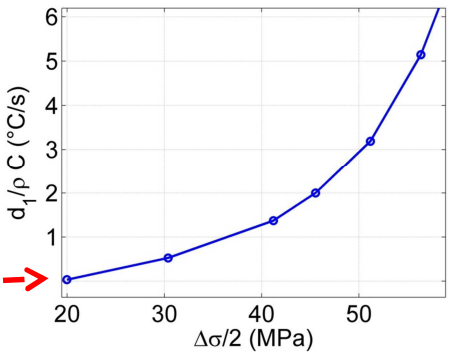

Figure 5- Zoom between 20 and 60 MPa

Figure 6 and 7 respectively show temperature and dissipation evolutions during fatigue tests (10^7 cycles) at 45 and 56 MPa. Temperature and dissipation always increased with the number of cycles. So no steady state was observed even at lower stress range (e.g. 20 MPa).

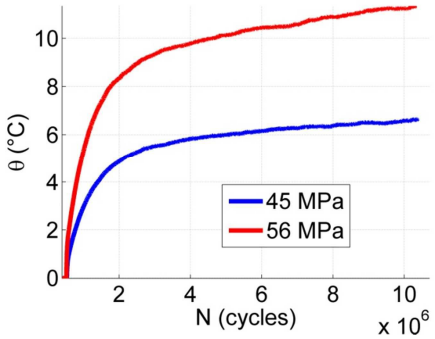

Figure 6- Temperature variation

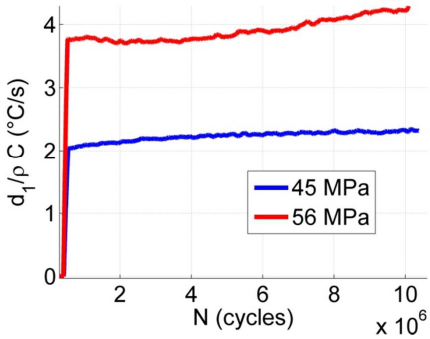

Figure 7- Dissipation

5. CONCLUSION

In this study, fatigue tests were performed at stress amplitude ranges much lower than fatigue strength. From temperature measurement, dissipated energy was determined using infrared thermal data and a 1D heat diffusion model. Results firstly showed that dissipation exists below the fatigue strength even at low stress amplitude (e.g. 20 MPa). Then, they showed that dissipation always increased with the number of cycles.

If we consider from a thermodynamic standpoint, that the fatigue limit exists when

- a stress threshold exists under which the material behaviour is purely reversible (i.e. no intrinsic dissipation),
- or a stabilized cyclic behaviour occurs where the mechanical cycles are irreversible thermodynamic cycles,

The results showed that there is no fatigue limit because neither elastic nor plastic shakedown occured.

6. ACKNOWLEDGEMENT

The authors wish to thank Agence Nationale de la Recherche France ANR-09-BLAN-0025-01 for their financial support in the framework of the ANR project DISFAT.

7. REFERENCES

1. Bathias, C. & Paris, P.Dekker., M., ed. (2004), *Gigacycle fatigue in mechanical practice*, CRC Press.

2. Stanzl-Tschegg, S.; Mughrabi, H. & Schoenbauer, B. (2007), 'Life time and cyclic slip of copper in the VHCF regime', *International Journal of Fatigue* **29**(9-11), 2050 - 2059.
3. Phung, N. L. (2012), 'Fatigue sous très faibles amplitudes de contrainte : Analyse des mécanismes précurseurs de l'amorçage de fissure dans le cuivre polycristallin', Thèse de doctorat, ENSAM Paris.
4. Honorat, V.; Moreau, S.; Muracciole, J.-M.; Wattrisse, B.; Chrysochoos, A.; (2005), *Calorimetric analysis of polymer behaviour using a pixel calibration of an IRFPA camera*, Int. J. on Quantitative Infrared Thermography, **2**(2),153-172.
5. Boulanger, T.; Chrysochoos, A.; Mabru, C. & Galtier, A. (2004), 'Calorimetric analysis of dissipative and thermoelastic effects associated with the fatigue behavior of steels', *International Journal of Fatigue* **26**(3), 221 - 229.
6. Doudard, C.; Calloch, S.; Hild, F. & Roux, S. (2010), 'Identification of heat source fields from infra-red thermography: Determination of 'self-heating' in a dual-phase steel by using a dog bone sample', *Mechanics of Materials* **42**, 55 - 62.